Chemosphere 291 (2022) 133054

Contents lists available at ScienceDirect

Chemosphere

journal homepage: www.elsevier.com/locate/chemosphere

Glycerol-assisted degradation of dibenzothiophene by *Paraburkholderia* sp. C3 is associated with polyhydroxyalkanoate granulation

Camila A. Ortega Ramírez, Travers Ching, Brandon Yoza, Qing X. Li *

Department of Molecular Biosciences and Bioengineering, University of Hawaii at Manoa, Honolulu, HI, USA

HIGHLIGHTS

- Glycerol enhanced degradation of dibenzothiophene (DBT) in *Paraburkholderia* sp. C3.
- Glycerol induced DBT cometabolism, revealed via proteomic profiling.
- Glycerol fed into lipid metabolism promoting polyhydroxyalkanoate (PHA) granule accumulation.
- 2-Bromoalkanoic acid inhibited PHA granule formation and the glycerol-enhanced DBT degradation in C3.

GRAPHICAL ABSTRACT

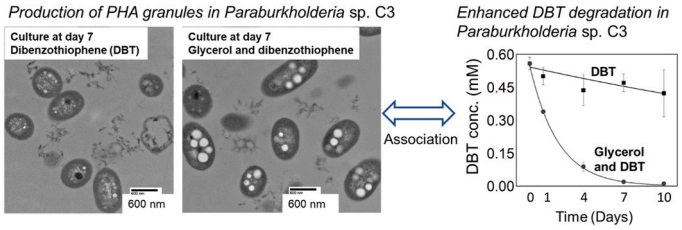

ARTICLE INFO

Handling Editor: Yongmei Li

Keywords:
Biodegradation
Biowaste
Dibenzothiophene
Glycerol
Lipid synthesis
Paraburkholderia
Polyhydroxyalkanoate

ABSTRACT

Glycerol is a biodiesel byproduct. In the present study, glycerol was used as a co-substrate during biodegradation of dibenzothiophene (DBT) by *Paraburkholderia* sp. C3. Polycyclic aromatic hydrocarbons (PAHs) are a group of persistent, ubiquitous and carcinogenic chemicals found in the environment. DBT is a major sulfur-containing PAH. The chemical properties of DBT make it an ideal model pollutant for examining the bioremediation of higher molecular weight PAHs. Bioremediation uses microbial catalysis for removal of environmental pollutants. Environmental microorganisms that encounter aromatic substrates such as heterocyclic PAHs develop unique characteristics that allow the uptake and assimilation of these cytotoxic substrates. Microbial adaptations include changes in membrane lipid composition, secretion of surface-active compounds and accumulation of lipid granules to withstand chemical toxicity. Biostimulation using more readily metabolized substrates can increase the biodegradation rate of PAHs, but the molecular mechanisms are not well understood. We analyzed the DBT biodegradation kinetics in C3, proteome changes and TEM micrographs in different culturing conditions. We utilized 2-bromoalkanoic lipid metabolic inhibitors to establish a correlation between polyhydroxyalkanoate (PHA) granule formation and the enhancement of DBT biodegradation induced by glycerol. This is the first description linking PHA biosynthesis, DBT biodegradation and 2-bromoalkanoic acids in a *Paraburkholderia* species.

1. Introduction

Polycyclic aromatic hydrocarbons (PAHs) are planar aromatic molecules composed of carbon and hydrogen atoms. Sulfur substitutions in PAHs distort planarity of the molecules, resulting in more reactive and carcinogenic heterocyclic PAHs (Dabestani and Lvanov 1999). After carbon and hydrogen, sulfur is the most abundant element in PAHs, existing in organic and inorganic fractions (Soleimani et al., 2007). A

* Corresponding author.
E-mail address: qingl@hawaii.edu (Q.X. Li).

https://doi.org/10.1016/j.chemosphere.2021.133054
Received 4 October 2021; Received in revised form 6 November 2021; Accepted 22 November 2021
Available online 25 November 2021

major component in organic fractions is dibenzothiophene (DBT), followed by benzothiophene, benzonaphthothiophenes and their alkylated homologs (Li et al., 2012). DBT is a hydrophobic heterocyclic PAH; its recalcitrant properties allow it to ubiquitously concentrate in the environment (Seo et al., 2009). Consequently, DBT is typically used as a model chemical to study spatial distribution and quantification of thermodynamically stable sulfur-containing PAHs (Li et al., 2012). The chemical properties of DBT also make it an applicable model pollutant for bioremediation of higher molecular weight PAHs (Nzila et al., 2018) and other aromatic environmental pollutants.

Bioremediation uses microbial catalysis for the removal of environmental pollutants. Two main factors affect PAH biodegradation efficiency: an appropriate microbial consortium (Szulc et al., 2014) and ample available organic carbon to support microbial growth (Tyagi et al., 2011). Environmental microorganisms encountering aromatic substrates such as heterocyclic PAHs develop unique characteristics allowing for the uptake and assimilation of these cytotoxic substrates (Di Martino et al., 2014). Adaptations that improve bioavailability include changes in membrane lipid composition to increase hydrophobicity and fluidity of outer membranes (Pini et al., 2009) and secretion of surface-active compounds (e.g., biosurfactants) that interact with non-conventional substrates (e.g., PAHs) to render them more bioavailable (Patowary et al., 2017). Within the cell, accumulation of lipid granules were shown to enable bacteria to better withstand chemical toxicity (Venkateswar Reddy et al., 2015; Cavaliere et al., 2018).

Supplementation with co-substrates is a strategy to induce adaptive pathways in biodegrading bacteria. For example, addition of glycerol – a biodiesel byproduct with versatile functions in microbial cells – enhanced DBT biodegradation 18-fold in *Paraburkholderia* sp. C3 (previously *Burkholderia* sp. C3) (Ortega Ramirez et al., 2020). Glycerol supplementation induced rhamnolipid (RL) biosynthesis and accelerated bacterial growth. Proteomic analysis revealed that β-oxidation and *de novo* synthesis of fatty acids (FAS II) pathways were involved (Ortega Ramirez et al., 2020), which was later supported by total genomic sequencing of C3 and DBT biodegradation experiments (Cao et al., 2021). Glycerol readily enters β-oxidation and FAS II pathways producing the lipid precursor for RL biosynthesis, R-3-hydroxydecanoyl-CoA, which is also a precursor in the biosynthesis of polyhydroxyalkanoates (PHAs) (Choi et al., 2011). This study associates the accumulation of PHA granules upon addition of glycerol into the culture media with enhancement biodegradation of DBT by *Paraburkholderia* sp. C3. It also furthers the understanding of the mechanisms involved in bacterial adaptation to non-conventional substrates such as PAHs.

PHAs are accumulated as intracellular granules (Lu et al., 2009). The accumulation of PHA granules has been described under metabolic stress conditions (Di Martino et al., 2014) and for energy storage (Rehm et al., 2001). PHAs can protect cells from phenolic microbial inhibitors such as catechol (Obruca et al., 2021). Catechol is a metabolite in the DBT oxidation pathway (Li et al., 2019). We hypothesized that PHA granules facilitate glycerol-enhanced DBT biodegradation in C3. This hypothesis was tested by inhibiting PHA precursor biosynthesis with 2-bromohexanoic acid (HEX) and 2-bromooctanoic acid (OC) (Gutierrez et al., 2013), and analyzing the inhibitors' impact on bacterial growth, DBT degradation kinetics, proteomic profiles, and PHA granule formation.

2. Materials and methods

2.1. C3 cultivation and DBT biodegradation

We followed methods previously described (Ortega Ramirez et al., 2020). Briefly, C3 cells were grown overnight in LB rich medium, washed three times, adjusted to 0.5 OD_{600}, and inoculated to a concentration of approximately 0.05 OD_{600} in five ml of minimal medium (MM) (Bastiaens et al., 2000) containing 50 mM glycerol and 0.54 mM (100 ppm) DBT in a test tube. The final concentrations of HEX and OC were 2 mM and 5 mM. Growth curves of C3 cultured with glycerol, but without DBT were also prepared (Fig. 1). All cultures were incubated in a rotary shaker at 30 °C and 200 rpm. The extraction and analysis of DBT were performed as previously described (Akhtar et al., 2009). Briefly, after culture acidification to pH 2–3 with HCl, DBT was extracted three times with ethyl acetate. Analysis was on an Agilent 1100 series high performance liquid chromatograph (HPLC) equipped with an Aqua C18 column (150 × 4.60 mm, 5 μm particle size; Phenomenex, Inc.). DBT was detected at 245 nm.

2.2. Data calculation

We followed methods previously described (Ortega Ramirez et al., 2020). Measured concentrations of DBT were averaged for each timepoint and the standard errors of the mean (SEM) representing variations among 3 or 6 biological replicates were calculated. Time points were fitted with a first-order kinetic equation, $C = C_0 \times e^{-kt}$. DBT half-life ($t_{1/2}$) was calculated as $t_{1/2} = \frac{\ln 2}{k}$. Multifactorial analysis of variance (ANOVA) with unequal sample sizes (n, 15 or 30) was used to calculate statistical significance (p-value < 0.05) using IBM SPSS Statistics 19 software. The p-value was set to 0.001 when the null hypothesis of homogeneity of variances was rejected. Least significant difference (LSD) and Tukey's honestly significant difference (HSD) post hoc tests were used for further exploration of the results. The fixed factors analyzed were type of inhibitor (OC, HEX or without; 3 levels), concentration (0, 2 or 5 mM; 3 levels) and incubation time (5 levels). The statistical model is provided in Suplemental information 1.

2.3. Protein extraction

C3 cells were collected from cultures at day two and washed three times with Milli-Q (mQ) water. Proteins were then extracted according to previously reported methods (Dephoure and Gygi, 2011) with modifications (Ortega Ramirez et al., 2020). Briefly, cell pellets were resuspended in lysis buffer consisting of 9 M urea and a protease inhibitor cocktail (Sigmafast™ Protease Inhibitor Cocktail Tablet, Sigma-Aldrich, Milwaukee, WI, USA). Cell membranes were then disrupted with six cycles of bead-beating at maximum speed for 60 s on a mini-beadbeater (BioSpec Products, Bartlesville, OK, USA); cells were put on ice for 60 s between each bead-beating cycle. Cell debris was removed by centrifugation. Proteins were concentrated with an Amicon Ultra-0.5 ml centrifugal filter (3K cut-off; Millipore, Bay City, MI, USA). Proteins (36 μg) were separated by 12% SDS-PAGE and visualized with Coomassie blue.

2.4. Protein sample preparation and liquid chromatography-tandem mass spectrometry (LC-MS/MS)

From each gel lane, 12 to 14 gel slices (1 mm^3) were washed with 25 mM ammonium bicarbonate (NH_4HCO_3)/50% acetonitrile (ACN) until gel pieces became clear. The protein disulfide bonds were reduced with dithiothreitol (DTT) at 56 °C for 30 min. The exposed cysteine residues were alkylated with iodoacetamide (IAA) at ambient temperature for 20 min. Gel pieces were dehydrated with 100% ACN prior to the DTT reduction and IAA alkylation steps. An in-gel protein digestion was done with Trypsin/Lys-C Mix, Mass Spec Grade (Promega, Fitchburg, WI, USA) at 37 °C for 16–18 h. The fractions of alkylated and reduced peptides were collected from the gel by centrifugation and then were desalted and concentrated with Pierce C18 tips (Thermo Scientific, Waltham, MA, USA).

Peptides were analyzed on a Bruker nanoLC-amaZon speed ion trap mass spectrometer system (Bruker Daltonics, Billerica, MA, USA). nanoLC separations were on a C18 analytical column (0.1 × 150 mm, 3

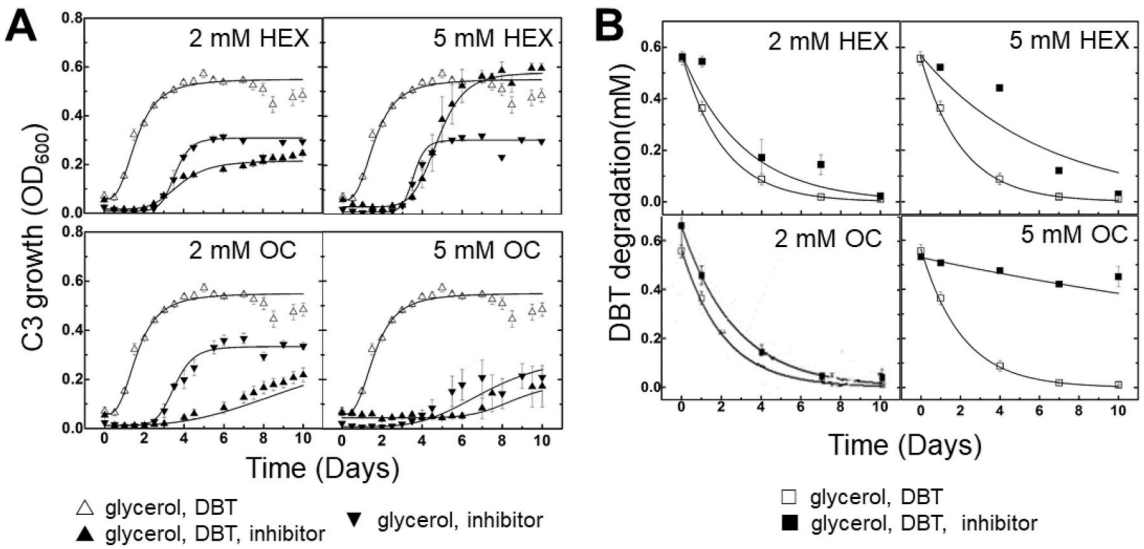

Fig. 1. Inhibition of PHA granule formation by OC decreased DBT biodegradation and C3 growth. All cultures contained 50 mM glycerol. The final concentrations of the 2-bromoalkanoic acids, OC and HEX, were 2 mM and 5 mM. An exponential decay equation, $C = C_0 \times e^{-kt}$, was used for fitting data points. Error bars represent variations among 3 or 6 samples. Inhibitors significantly affected DBT degradation ($p < 0.001$). HEX, 2-bromohexanoic acid; OC, 2-bromooctanoic acid.

μ, 200 Å, Bruker Daltonics) with gradient elution from 5% to 65% ACN in 0.1% formic acid for 80 min after a 2-min running delay. After elution, the mobile phase was switched to 95% ACN in 0.1% formic acid for 10 min, and then to 5% ACN in 0.1% formic acid for 20 min to equilibrate the column. The flow rate was 800 nl/min. The mass spectrometer parameters were set at a capillary voltage of 1600 V and a capillary temperature of 149.5 °C. A survey scan from *m/z* 400–3000 was followed by data-dependent MS/MS acquisition of the 10 most abundant ions and 0.5 Da instrument error. Dynamic exclusion was set to repeat the same precursor ion twice, followed by excluding it for 0.8 min.

2.5. Protein database search

Raw files (file type BAF) were converted to mascot generic format (mgf) with DataAnalysis software (Bruker Daltonics). Apex was used as the peak picking algorithm with 100 as the absolute intensity threshold. Parameters for finding MS and MS/MS compounds were selected based on the capabilities of the instrument. The protein database, containing canonical and isoform protein sequences from *Burkholderia* [UniProt taxonomy: 32008], was downloaded in FASTA format from the UniProt Knowledgebase (April 4, 2016 at 9:35 a.m.). The database search was conducted with MyriMatch (Tabb et al., 2008). The search parameters were set to ion trap for instrument type, auto for precursor mass, trypsin/P for enzyme, *m/z* 0.5 for both precursor and fragment tolerance. Modifications were carbamidomethyl (fixed) and methionine oxidation (variable).

2.6. Data normalization

Spectral counts of proteins identified (by peptide assignment) in each treatment were obtained with IDPicker 3.0 (Ma et al., 2009). Filters to match peptides with their MS/MS spectra were: Maximum false discovery rate (FDR) of 1% and minimum one spectrum per peptide and per match. In order to match peptides to proteins, a minimum of two distinct peptides and spectra and a minimum of one additional peptide were allowed (Tabb et al., 2008; Ma et al., 2009). Data were normalized according to (Griffin et al., 2010) with the assumption that MS/MS intensities are equal to one regardless of the peptide length. A log (normalized count + 1) was applied, and the normalized data files were compared to the raw ones. Treatments were: A, 0.54 mM DBT; B, 50 mM glycerol; C, 50 mM glycerol and 0.54 mM DBT; and D, 50 mM glycerol, 0.54 mM DBT and 2 mM OC. The calculated relative abundance of each protein was averaged for biological triplicates in each treatment. The normalized relative abundance of each protein identified in the different conditions and their *p*-value is provided in Supplemental information 2.

2.7. Transmission electron microscopy (TEM)

Specimens were fixed with 2.5% glutaraldehyde and 0.1 M calcium chloride in 0.1 M sodium cacodylate buffer, pH 7.2 for a week, washed in 0.1 M cacodylate buffer twice for 30 min each time, followed by post fixation with 1% OsO_4 in 0.1 M cacodylate buffer for 1 h. Cells were dehydrated in a graded ethanol series (30%, 50%, 70%, 85%, 95% and 100%), substituted with propylene oxide and embedded in LX112 epoxy resin. Ultrathin (60–80 nm) sections were obtained on an RMC PowerTome ultramicrotome, double stained with uranyl acetate and lead citrate, viewed on a Hitachi HT7700 TEM at 100 kV and photographed with an AMT XR-41B 2k x 2k CCD camera.

3. Results and discussion

3.1. Glycerol-enhanced DBT biodegradation is inhibited by 2-bromoalkanoic acids in C3

Significant differences in DBT degradation by C3 were attributed to inhibitor concentration ($p < 0.001$) rather than to the inhibitor alkyl-chain length (C_6 *vs* C_8): Our statistical model (Supplemental information 1, Adjusted $R^2 = 0.917$) associated a 58.9% effect to the inhibitor concentration (0, 2 or 5 mM) and a 14.2% effect to the type of inhibitor (none, HEX, OC) (Fig. 1B).

A 2 mM inhibitor concentration decreased the DBT biodegradation rate constant from 0.479 day^{-1} with no inhibitors to 0.324 day^{-1} with HEX, and to 0.374 day^{-1} with OC (Table 1). At 5 mM, the rate constant decreased from 0.479 to 0.162 day^{-1} with HEX and to 0.033 day^{-1} with OC (Table 1).

Unlike the biodegradation of DBT by C3, both the type of inhibitor and the inhibitor concentration influenced C3 growth (Fig. 1A). When C3 cells were cultured in 50 mM glycerol and 0.54 mM DBT (no inhibitor), growth reached an OD_{600} of 0.55 at day 4. When the inhibitors were added, C3 growth reached an OD_{600} of 0.19 with 2 mM HEX and an OD_{600} of 0.56 with 5 mM HEX by day 7. The opposite was observed for

Table 1
Influence of 2-bromoalkanoic acid inhibitors on the DBT biodegradation rate constant and DBT half-life. An exponential decay equation, $C = C_0 \times e^{-kt}$, was used for fitting "N" data points, where k is rate constant and t is time in days. Fold-change was relative to the rate constant of cultures grown with 50 mM glycerol & 0.5 mM DBT. [a] Relative to DBT alone.

Treatment	Rate constant (Day^{-1})	R^2	Half-life (Day)	N	Fold change
50 mM glycerol & 0.5 mM DBT	0.479 ± 0.02	0.99	1.6	30	18.0[a]
2 mM HEX, 50 mM glycerol & 0.5 mM DBT	0.324 ± 0.00	1.00	2.1	15	11.8
2 mM OC, 50 mM glycerol & 0.5 mM DBT	0.374 ± 0.03	0.97	1.9	30	13.8
5 mM HEX, 50 mM glycerol & 0.5 mM DBT	0.162 ± 0.05	0.88	4.3	15	5.4
5 mM OC, 50 mM glycerol & 0.5 mM DBT	0.032 ± 0.00	0.98	215	15	0.3

the biodegradation of DBT. C3 cells grown with 2 mM HEX had higher degradation levels at day 4 as compared with those cultivated with 5 mM HEX. It is interesting that 2 mM HEX had a greater effect on C3 growth than its DBT biodegradation ability. C3 growth at 2 and 5 mM OC achieved 0.13 and 0.08 OD_{600}, respectively, by day 7 and further increased by day 10. These observations suggest that glycerol-enhanced co-metabolism is the result of several metabolic mechanisms and not only those involved with increased C3 biomass.

The effects of HEX and OC on C3 growth in cultures supplemented with 50 mM glycerol in the absence of DBT were also studied (Fig. 1A). C3 cells grew equally with 2 mM and 5 mM of HEX. Unlike with HEX, 5 mM of OC decreased C3 growth compared to 2 mM of OC. A 2 mM OC concentration was selected as the DBT degradation inhibitor for proteome profiling experiments because the inhibition of DBT degradation was transient in the presence of 2 mM of OC and the degradation kinetics was similar to the one in the absence of inhibitor.

3.2. The global correlation of the C3 proteome treated with OC resembles the one with DBT alone

A total of 1935 proteins were identified with a 0.03% FDR (Supplemental information 2). Within each treatment, identified proteins were consistent among biological triplicates. The global effects of each treatment are shown with the PCA plot in Fig. 2.

The global proteome from C3 grown with 50 mM glycerol and 0.54 mM DBT (Treatment C) clustered on the PC1 axis with the proteome from C3 grown with 50 mM glycerol (Treatment B), whereas the global proteome from C3 grown with 50 mM glycerol, 0.54 mM DBT and 2 mM OC (Treatment D) clustered along the PC1 axis with the proteome from cells grown in the 0.54 mM DBT treatment (Treatment A). Thus, OC appeared to reduce the influence of glycerol supplementation on global proteome profiles.

The individual proteins showing significant differences (Supplemental information 3, adjusted p-value < 0.05) in relative abundances of the confidently identified 1935 proteins were compared in a heat map (Fig. 3). This analysis reached similar conclusions to the PCA analysis. The proteome of C3 exposed to OC behaves similarly to the one exposed to DBT at the global (Fig. 2) and local levels (Fig. 3) of correlation.

3.3. Glycerol assimilation is delayed by the OC inhibitor

In treatments B (50 mM glycerol) and C (50 mM glycerol and 0.54 mM DBT), upon uptake, possibly by GlpF (not detected; however, *GlpF* detected in chromosomes 2, Cao et al., 2021), glycerol underwent

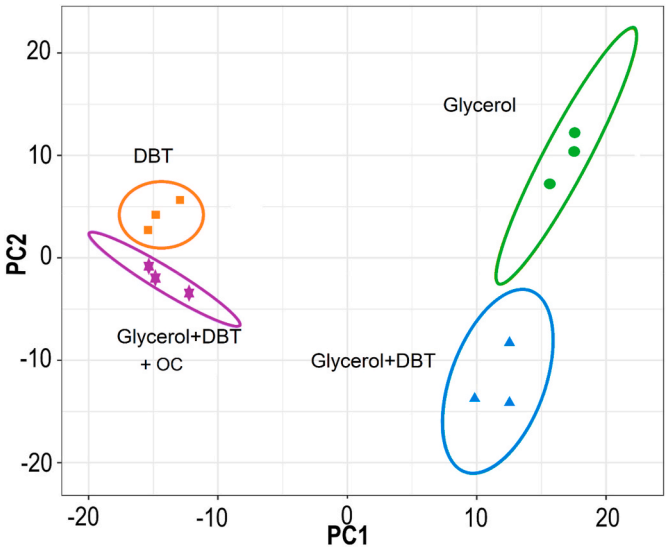

Fig. 2. The proteome of *Paraburkholderia* sp. C3 exposed to 2 mM OC clustered closer to the one exposed to DBT alone. DBT, dibenzothiophene; OC, 2-bromooctanoic acid.

phosphorylation by GlpK (UniProtID: A0A0D5VFT7) followed by conversion to dihydroxyacetone-3-phosphate by GlpD (UniProtID: A0A0D5VFY1) and entered glycolysis or gluconeogenesis as D-glyceraldehyde-3-phosphate (Table 2). This supported cell growth and consequently enhanced DBT biodegradation (Fig. 1). C3 also assimilated glycerol as glycerate-3-phosphate by glycerate kinase (GK) (UniProtID: A0A0D5VC54) when C3 was cultured with glycerol (Treatment B) or the DBT/glycerol mixture (Treatment C) (Table 2). However, the relative abundances of GK were lower than those of GlpD (UniProtID: A0A0D5VFY1) and GlpK (UniProtID: A0A0D5VFT7). Glycerol assimilatory proteins GlpD and UspC (UniProt ID: A0A0D5V9F3) were only detected in treatments with glycerol biostimulation (Treatments B and C). Interestingly, these proteins (GlpD, UspC) were not detected in treatment D, indicating that the OC inhibitor prevented glycerol assimilation at day 2 of incubation. The UgpC subunit was detected in treatments B and C (Table 2). UgpC is the ATP binding subunit of UgpBAEC, an ABC-type transporter involved in glycerol-3-phosphate import that supplies the cell with organic bound phosphate (Blank, 2012).

3.4. Glycerol biostimulation induced DBT biodegradation enzymes in C3

The results suggest that a cometabolism phenomenon occurred with DBT, a non-conventional substrate that provides neither energy or nutrients, and glycerol, a conventional carbon source. This phenomenon has been described for other non-conventional substrates (Wackett, 1996). Moreover, the results indicate that glycerol induced accumulation of catabolic enzymes contrary to the laws of cell metabolic efficiency (Table 2, Fig. 4: Treatment B). The only aromatic-catabolizing enzymes involved in degradation of DBT and other xenobiotics (e.g., naphthalene and phenanthrene) that were not detected in Treatment B were naphthalene-1,2-dioxygenase (UniProt ID: A0A0M4NP56), DbtAd (UniProt ID: Q93NA7), PhnD (UniProt ID: C7DQZ8) and catechol-2, 3-dioxygenase (UniProt ID: Q9RB89). Our proteomics data set is an example of cometabolism for bacterial growth, in which the conventional substrate may also function to induce several catabolic enzymes for degradation of the non-conventional substrate (Elliot et al., 2010).

Proteins specifically involved in DBT degradation were identified in C3 (Fig. 4; Table 2). Fig. S1 shows the putative catalytic steps of these enzymes from initial deoxygenation to acetal production (DbtA-cAdBCDE). The protein cluster was initially observed in *Burkholderia*

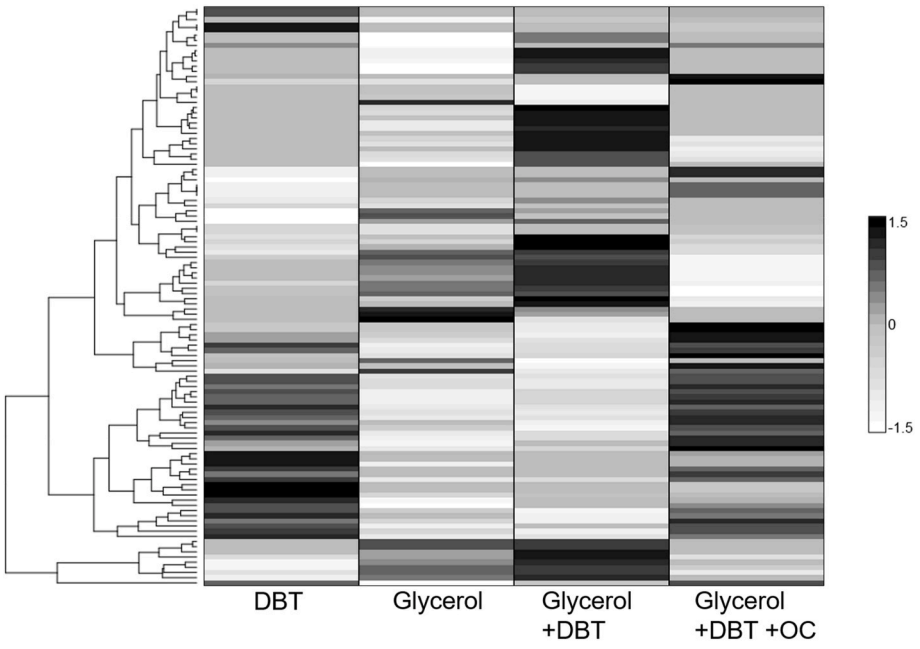

Fig. 3. Individual proteins profiles with significant differences in relative abundance (Adjusted $p > 0.05$) exposed to DBT are similar to those exposed to OC inhibitor. DBT, dibenzothiophene; OC, 2-bromooctanoic acid.

fungorum sp. DBT1 (Di Gregorio et al., 2004; Piccoli et al., 2014).

The identified enzymes, DbtAcAdBCE (Table 2), evidenced that C3 degrades DBT through lateral deoxygenation, also known as the Kodama pathway (Kodama et al., 1973). The first and most important step in this pathway is mediated by a two-subunit DBT dioxygenase composed of DbtAc and DbtAd (Fig. 4, Table 2). Bacteria with a mutated DBT dioxygenase lose their ability to metabolize DBT (Denome et al., 1993; Di Gregorio et al., 2004). Ring-hydroxylating dioxygenases incorporate molecular oxygen at PAH positions 1,2; 3,4 or 9,10. Deoxygenation is necessary for ortho-, meta- and para-cleavage of the aromatic ring. The position of oxygen incorporation depends on the dioxygenase specificity (Seo et al., 2007; Gao et al., 2013). The metabolites produced are therefore dependent on the initial deoxygenation reaction.

Phn and Nag-like aromatic catabolic enzyme clusters identified previously in C3 for phenanthrene and naphthalene degradation (Tittabutr et al., 2011) were detected in all treatments. Detection of phenanthrene and naphthalene dioxygenase subunits (Table 2, UniProt ID: C7DR00 and A0A0M4NP56, respectively) suggested the potential for broad enzyme specificity towards DBT degradation. This mechanism was independent of glycerol biostimulation as the dioxygenases were detected in treatment A (DBT alone) as well as in treatments B, C and D (in the presence of glycerol). Phenanthrene is a 3-ring PAH with an octanol/water partitioning coefficient (logP) that is similar to DBT (logP 4.46 *vs* 4.44 (Heipieper and Martínez, 2010)). Dioxygenases with broad specificity have been reported to degrade biphenyl, 2,4-dinitrotoluene and DBT (Kimura et al., 1997; Seo et al., 2011). Additionally, *E. coli* transformants containing *phn* and *nag*-like dioxygenase genes partially degraded DBT (Tittabutr et al., 2011) and may share a crossover metabolic point between phenanthrene and DBT in *Mycobacterium aromaticivorans* JS19b1^T (Seo et al., 2011). Our proteomic results indicated that DBT, phenanthrene and naphthalene may undergo crossover pathways in C3.

Catechol 2,3-dioxygenase (UniProt ID: Q9RB89) was detected in treatments A and D, but not in treatments B and C. Catechol 2,3-dioxygenase degrades catechol into *cis, cis*-muconic acid (Fuchs et al., 2011). It is hypothesized that C3 grown with DBT alone converted salicylic acid into catechol and gentisate that were further converted into *cis, cis*-muconic acid and maleylpyruvic acid, respectively (Fig. 4). In treatments B and C, salicylic acid was fully converted into maleylpyruvic acid. These changes suggest that glycerol biostimulation may reduce metabolite cytotoxicity (George and Hay, 2012). Catechol and gentisate metabolites were also observed in the carbaryl biodegradation pathway in C3 (Seo et al., 2013).

3.5. Glycerol induced PHA granule biosynthesis in C3

Glycerol entered the lipid metabolic pathways in C3 as indicated by detection of proteins related to the FAS II pathway (Table 2). Additionally, significant abundances of phasins (UniProt ID: A0A0N1KL01 and A0A0D5VHK5), multifaceted PHA granule-associated proteins, suggest that C3 forms PHA granules upon cultivation with glycerol, glycerol/DBT (Table 2: Treatments B, C and D) and DBT alone (Table 2: Treatment A). Phasins attach to granules serve a role in PHA volume-to-surface ratio determination (Jendrossek, 2009) and stabilization (Jurasek and Marchessault, 2002), whereas poly(R)-hydroxyalkanoic acid synthase (UniProt ID: A0A0Q5H1G7, W6X074 and A9BZX2) and poly-beta-hydroxybutyrate polymerase (UniProt ID: D8P4I5) catalyze granule formation and aggregation (Lu et al., 2009). PHA granule formation suggests lipid storage when a high concentration of carbon source is available (Rehm et al., 2001). Interestingly, some of these proteins (e.g., phasins) were also observed in C3 cultured with DBT alone, which would be considered a carbon limiting condition. However, the abundances of enzymes responsible for granule formation and aggregation were much higher when glycerol was used as a co-substrate than when DBT was the only carbon source. The findings support that glycerol biostimulation increased PHA granule formation in C3 (Table 2). PAHs such as phenanthrene and naphthalene have been observed to attach to PHA granules (Cavalier et al., 2018) possibly denoting a slow PAH release mechanism that would potentially reduce their toxicity. PHA accumulation has been described as a stress response in several microorganisms such as *Pseudomonas* and stress factors such as osmotic and oxidative pressure (Obruca et al., 2021). It is apparent that DBT causes toxicity stresses to C3 cells, which is a probable cause of PHA accumulation.

Lastly, abundances of cyclopropane-fatty-acyl-phospholipid synthase (UniProt ID: A0A0D5VF95), involved in formation of cyclopropane membrane fatty acids from S-adenosyl-L-methionine and phospholipid olefinic, and phosphatidylethanolamine-binding family

Table 2
C3 protein profiles involved in glycerol assimilation, DBT biodegradation, PHA synthesis and PHA granule formation. ND: Not detected. Treatments were: A, 0.54 mM DBT; B, 50 mM glycerol; C, 50 mM glycerol and 0.54 mM DBT; D, 50 mM glycerol, 0.54 mM DBT and 2 mM OC. Proteins were extracted on day 2. Three biological replicates were analyzed in each treatment.

UniProt ID	Protein description (name)	Relative abundance by treatment				
		Metabolic function	A	B	C	D
G5L3J5	Hydratase aldolase (DbtE)[a]	DBT degradation	1.98	1.27	2.33	2.40
Q93CN9	Extradiol dioxygenase (DbtC)	DBT degradation	1.82	0.96	1.43	1.91
Q93CN7	Putative monooxygenase α- subunit		2.02	1.62	2.02	1.87
Q93NA7	Dioxygenase β- subunit (DbtAd)[a]	DBT degradation	1.83	ND	1.83	2.30
Q93NA6	Dihydrodiol dehydrogenase (DbtB)	DBT degradation	1.63	0.88	1.28	1.35
Q93CN6	Putative hydrolase		0.97	1.09	0.93	1.30
Q93NA8	Dioxygenase α- subunit (DbtAc)	DBT degradation	1.59	1.00	1.44	1.60
C7DQZ5	Dehydrogenase (PhnF)	Phenanthrene degradation	1.03	1.08	1.23	0.74
C7DQY7	*Cis*-naphthalene dihydrodiol dehydrogenase (NahB)	Naphthalene degradation	1.49	1.64	1.46	1.13
C7DQY6	PAH dioxygenase small subunit[a]	PAH degradation	1.45	1.40	1.12	0.92
C7DQY8	Salicylaldehyde dehydrogenase (NagF)	Naphthalene degradation	1.38	1.24	1.82	1.96
C7DQY1	Ferredoxin reductase (NagAa)	Salicylic acid degradation	1.32	1.36	1.36	1.34
C7DQZ1	Gentisate-1,2-dioxygenase (NagI)	Gentisate degradation	1.40	1.09	1.12	1.20
C7DR01	Dihydrodiol dehydrogenase (PhnB)	Phenanthrene degradation	1.17	1.06	1.13	0.82
C7DQZ7	Extradiol dioxygenase (PhnC)	Phenanthrene degradation	1.34	0.95	1.38	1.20
C7DQY5	PAH dioxygenase large subunit	PAH degradation	1.31	0.76	1.30	1.10
C7DQZ6	Hydratase/aldolase (PhnE)	Phenanthrene degradation	ND	0.75	1.19	1.30
C7DQY9	1,2-Dihydroxynaphthalene dioxygenase (NahC)	Naphthalene degradation	1.23	ND	ND	1.24
C7DQZ2	Fumarylacetoacetate hydrolase		0.72	0.79	0.70	0.53
C7DQZ0	Reductase component of salicylate-5-hydroxylase (NdsA)		1.02	0.75	1.05	0.41
C7DQZ3	Salicylate-5-hydroxylase large oxygenase component (NagG)	Salicylic acid degradation	ND	1.01	1.29	0.69
C7DR00	Dioxygenase β-subunit (PhnAd)	Phenanthrene degradation	ND	0.60	ND	ND
C7DQZ8	Isomerase (PhnD)	Phenanthrene degradation	0.23	ND	0.44	0.53
R9W162	Aromatic-ring-hydroxylating dioxygenase[a]		1.73	0.42	1.58	2.17
Q9RB89	Catechol 2,3-dioxygenase[a]	Catechol degradation	1.71	ND	ND	1.44
A0A0M4NP56	Naphthalene-1,2-dioxygenase[a]	Naphthalene degradation	1.68	ND	1.66	1.76
A0A0D5VFY1	Glycerol-3-phosphate dehydrogenase (GlpD)[a]	Glycerol utilization	ND	1.07	1.94	ND
A0A0D5V9F3	sn-glycerol-3-phosphate import ATP-binding (UgpC)[a]	Glycerol utilization	ND	0.51	0.82	ND
A0A0D5VFT7	Glycerol Kinase (GlpK)[a]	Glycerol utilization	ND	1.54	1.46	ND
A0A0D5VC54	Glycerate kinase	Glycerol utilization	ND	0.86	0.46	ND
Q63S87	β-oxoacyl-ACP synthesis (FabF)	FASII pathway	ND	0.62	1.38	ND
A0A0D5VAR9	3-oxoacyl-ACP-reductase (FabG)	FASII pathway	1.32	1.06	1.36	1.45
A0A0D5VAC6	3-hydroxy -ACP-dehydratase (FabZ)	FASII pathway	0.98	ND	ND	1.10
K8R0G3	Acyl-CoA dehydrogenase (FadE)	β-oxidation	ND	ND	0.69	ND
Q3JVY2	Enoyl-CoA hydratase/3- hydroxyacyl-CoA dehydrogenase (FadB)	β-oxidation	ND	1.15	1.14	ND
A0A0Q5H1G7	Poly(R)-hydroxyalkanoic acid synthase[a]	PHA synthesis	0.23	0.00	0.83	0.80
W6X074	Poly(R)-hydroxyalkanoic acid synthase, class I[a]	PHA synthesis	0.41	0.00	0.54	0.95
A9BZX2	Poly(R)-hydroxyalkanoic acid synthase, class I[a]	PHA synthesis	0.00	0.13	0.83	0.80
D8P4I5	Poly-beta-hydroxybutyrate polymerase	PHA synthesis	0.23	0.37	0.49	1.05
A0A0D5VF95	Cyclopropane-fatty-acyl-phospholipid synthase		ND	0.95	1.52	0.26
A0A0N1KL01	Phasin family protein[a]	PHA granule accumulation	2.03	2.13	2.26	1.96
A0A0D5VHK5	Phasin family domain protein	PHA granule accumulation	ND	1.57	1.78	0.80
I7A5Y0	PHA synthesis regulatory protein (PhaR)	PHA synthesis regulation	0.94	0.42	0.46	0.26
A0A0D5VCV0	Phosphatidylethanolamine-binding family protein[a]		0.23	0.66	0.96	1.24

[a] The relative abundance among treatment showed significant differences (adjusted p-value < 0.05).

protein (UniProt ID: A0A0D5VCV0) suggested that glycerol provides C3 with a carbon supply for lipid changes to the cell membrane. Cyclopropane fatty acids were observed in response to organic solvent (Pini et al., 2009) and naphthalene tolerance (Adebusuyi and Foght, 2013) in *Pseudomonas* species.

3.6. 2-Bromoalkanoic acids delay glycerol-induced PHA granule formation in C3

C3 protein profiles suggested that enhanced PHA granule formation is associated with glycerol-enhanced DBT degradation. C3 cells cultured with DBT alone (Treatment A) did not have PHA granules at day 2 of incubation. Granules were observed at day 7 (data not shown), but only in a few cells (Fig. 5, DBT). On the contrary, PHA granules had formed by day 2 with glycerol supplementation, as observed by the white round vesicles inside the cells. A further increase in granulation was observed on day 7 of incubation (Fig. 5, glycerol and DBT). Finally, both HEX and OC at 2 mM inhibited PHA granule formation on day 2. Granulation was restored by day 7.

TEM sample preparation involves the fixing of cells into a solid support from which cross sections are cut, limiting the amount of information that can be obtained on the exact size of PHA granules. However, the trend was that smaller vesicles were observed at the earlier stage of incubation (Day 2), whereas bigger granules approximately 100–200 nm in diameter were observed at the later stage of incubation (Day 7). Cell membrane detachment of vesicles was also observed (Fig. 5, DBT) and was more noticeable in C3 cells cultured with DBT as the only carbon source. Altogether, PHA granule formation mediated glycerol-enhanced DBT degradation in C3.

4. Conclusion

Our study analyzed the molecular mechanisms involved in glycerol-enhanced DBT biodegradation by the *Paraburkholderia* species. Proteomics profiling in *Paraburkholderia* sp. C3 revealed catabolic enzymes that are specific for DBT biodegradation by cells supplemented with glycerol, denoting a cometabolism phenomenon. Changes in lower aromatic catabolism pathways for the production of less toxic metabolites and glycerol-enhanced PHA granules were observed and were associated with DBT biodegradation determined by the use of inhibitors during

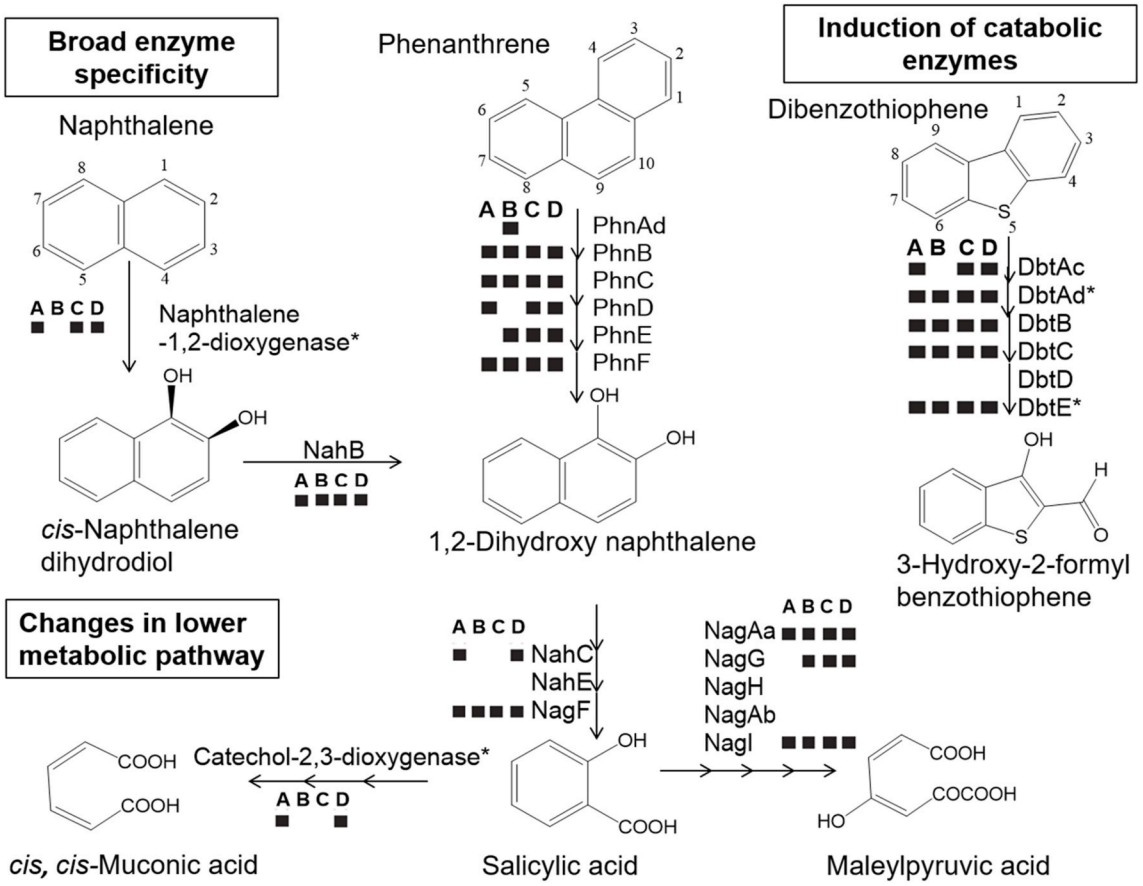

Fig. 4. Biostimulation with glycerol induced catabolic DBT degradation enzymes in *Paraburkholderia* sp. C3. Proteins with significant differences in relative abundance (Adjusted $p > 0.05$) are shown with *. DBT, dibenzothiophene.

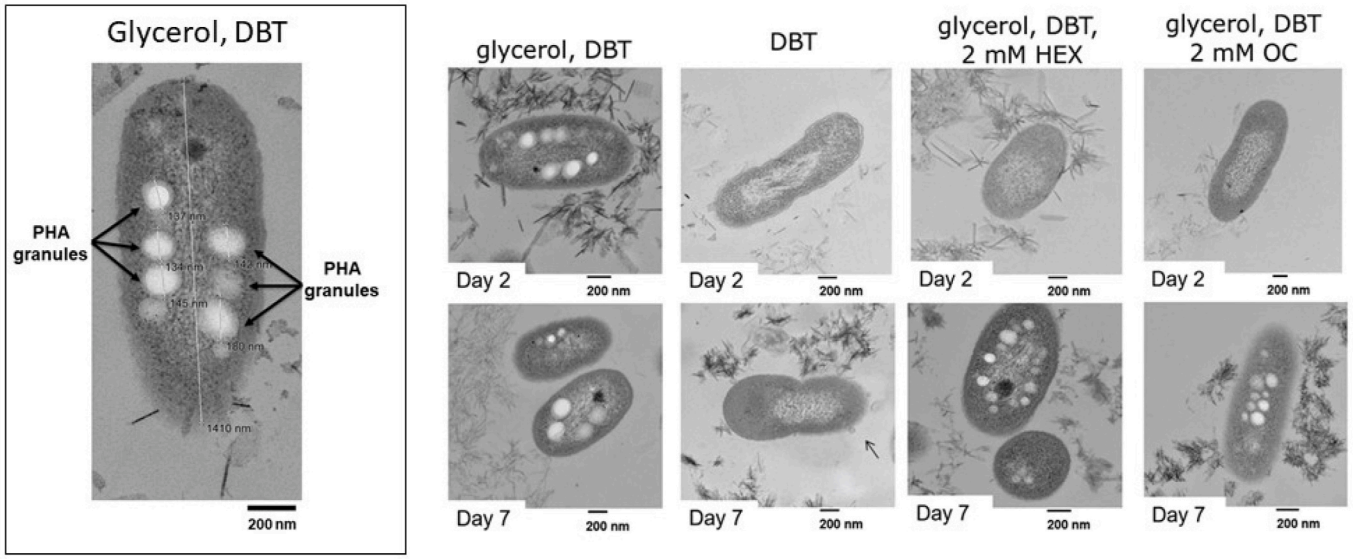

Fig. 5. Glycerol-induced PHA lipid vesicle formation in C3 was inhibited by HEX and OC. Cells were incubated with 0.54 mM DBT with or without 50 mM glycerol. Cell membrane vesicle detachment is shown with an arrow. DBT crystals were observed surrounding C3 cells. Micrographs were taken at days 2 and 7 of incubation. PHA vesicles were between 100 and 200 nm in diameter. HEX, 2-bromohexanoic acid; OC, 2-bromooctanoic acid; DBT, dibenzothiophene; PHA, polyhydroxyalkanoate.

DBT degradation kinetic experiments and TEM microscopy. Lastly, a protein involved in changes in the cell membrane fatty acid composition was detected when glycerol was the co-substrate, which may be partially responsible for an increased xenobiotic tolerance and bioavailability. Broad-enzyme specificity and metabolic pathway crossover was also suggested by the proteomic data, independent of glycerol

supplementation. The mechanisms described here may help with decision making in bioremediation of PAH-contaminated sites.

Credit author statement

Camila A. Ortega Ramirez: Conceptualization, Data curation, Formal analysis, Investigation, Methodology, Validation, Visualization, Writing - original draft. **Travers Ching:** Proteomics statistical analysis. **Brandon Yoza:** Funding acquisition. **Qing X. Li:** Conceptualization, Supervision, Project administration, Resources, Funding acquisition, Writing – review and editing.

Declaration of competing interest

The authors declare that they have no known competing financial interests or personal relationships that could have appeared to influence the work reported in this paper.

Acknowledgements

This work was supported in part by grant N00014-12-1-0496 from the Office of Naval Research and HAW05044R from the USDA. Authors thank Dr. Margaret Baker for helpful discussions and assistance with the mass spectral analysis of proteomics data.

Appendix A. Supplementary data

Supplementary data to this article can be found online at https://doi.org/10.1016/j.chemosphere.2021.133054.

References

Adebusuyi, A.A., Foght, J.M., 2013. The EmhABC efflux pump in *Pseudomonas fluorescens* LP6a is involved in naphthalene tolerance but not efflux. Appl. Microbiol. Biotechnol. 97, 2587–2596. https://doi.org/10.1007/s00253-012-4373-9.

Akhtar, N., Ghauri, M.a., Anwar, M.a., Akhtar, K., 2009. Analysis of the dibenzothiophene metabolic pathway in a newly isolated *Rhodococcus* spp. FEMS Microbiol. Lett. 301, 95–102. https://doi.org/10.1111/j.1574-6968.2009.01797.x.

Bastiaens, L., Springael, D., Wattiau, P., Verachtert, H., Harms, H., DeWachter, R., Diels, L., 2000. Isolation of adherent polycyclic aromatic hydrocarbon (PAH) -degrading bacteria using PAH-sorbing carriers. Appl. Environ. Microbiol. 66, 1834–1843. https://doi.org/10.1128/AEM.66.5.1834-1843.2000 (Updated).

Blank, L.M., 2012. The cell and P: from cellular function to biotechnological application. Curr. Opin. Biotechnol. 23, 846–851. https://doi.org/10.1016/j.copbio.2012.08.002.

Cao, J., Wang, W., Zhao, Z., Liu, X., Li, Q.X., 2021. Genome, metabolic pathways and characteristics of cometabolism of dibenzothiophene and the biodiesel byproduct glycerol in *Paraburkholderia* sp. C3. Bioresour. Technol. 326, 124699. https://doi.org/10.1016/j.biortech.2021.124699.

Cavaliere, C., Maria, C., Laura, A., La, G., Piovesana, S., Rotatori, M., Valentino, F., Laganà, A., 2018. Extraction of polycyclic aromatic hydrocarbons from polyhydroxyalkanoates before gas chromatography/mass spectrometry analysis. Talanta 188, 671–675. https://doi.org/10.1016/j.talanta.2018.06.038.

Choi, M.H., Xu, J., Gutierrez, M., Yoo, T., Cho, Y.H., Yoon, S.C., 2011. Metabolic relationship between polyhydroxyalkanoic acid and rhamnolipid synthesis in *Pseudomonas aeruginosa*: comparative 13C NMR analysis of the products in wild-type and mutants. J. Biotechnol. 151, 30–42. https://doi.org/10.1016/j.jbiotec.2010.10.072.

Dabestani, R., Lvanov, I.N., 1999. A compilation of physical, spectroscopic and photophysical properties of polycyclic aromatic hydrocarbons. Photochem. Photobiol. 70, 10–34. https://doi.org/10.1111/j.1751-1097.1999.tb01945.x.

Denome, S.a., Stanley, D.C., Olson, E.S., Young, K.D., 1993. Metabolism of dibenzothiophene and naphthalene in *Pseudomonas* strains: complete DNA sequence of an upper naphthalene catabolic pathway. J. Bacteriol. 175, 6890–6901. PMC206814.

Dephoure, N., Gygi, S.P., 2011. A solid phase extraction-based platform for rapid phosphoproteomic analysis. Methods 54, 379–386. https://doi.org/10.1016/j.ymeth.2011.03.008.

Di Gregorio, S., Zocca, C., Sidler, S., Toffanin, A., Lizzari, D., Vallini, G., 2004. Identification of two new sets of genes for dibenzothiophene transformation in *Burkholderia* sp. DBT1. Biodegradation 15, 111–123. https://doi.org/10.1023/B:BIOD.0000015624.52954.b6.

Di Martino, C., Catone, M.V., López, N.I., Raiger Iustman, L.J., 2014. Polyhydroxyalkanoate synthesis affects biosurfactant production and cell attachment to hydrocarbons in *Pseudomonas* sp. KA-08. Curr. Microbiol. 68, 735–742. https://doi.org/10.1007/s00284-014-0536-5.

Elliot, R., Singhal, N., Swift, S., 2010. Surfactants and bacterial bioremediation of polycyclic aromatic hydrocarbon contaminated soil – unlocking the targets. Crit. Rev. Environ. Sci. Technol. 41, 78–124. https://doi.org/10.1080/00102200802641798.

Fuchs, G., Boll, M., Heider, J., 2011. Microbial degradation of aromatic compounds- from one strategy to four. Nat. Rev. Microbiol. 9, 803–816. https://doi.org/10.1038/nrmicro2652.

Gao, S., Seo, J.S., Wang, J., Keum, Y.S., Li, J., Li, Q.X., 2013. Multiple degradation pathways of phenanthrene by *Stenotrophomonas maltophilia* C6. Int. Biodeterior. Biodegrad. 79, 98–104. https://doi.org/10.1016/j.ibiod.2013.01.012.

George, K.W., Hay, A., 2012. Less is more: reduced catechol production permits *Pseudomonas putida* F1 to grow on styrene. Microbiol. 158, 2781–2788. https://doi.org/10.1099/mic.0.058230-0.

Griffin, N.M., Yu, J., Long, F., Oh, P., Shore, S., Li, Y., Koziol, J.A., Schnitzer, J.E., 2010. Label-free, normalized quantification of complex mass spectrometry data for proteomic analysis. Nat. Biotechnol. 28, 83–89. https://doi.org/10.1038/nbt.1592.

Gutierrez, M., Choi, M.H., Tian, B., Xu, J., Rho, J.K., Kim, M.O., Cho, Y.H., Yoon, S.C., 2013. Simultaneous inhibition of rhamnolipid and polyhydroxyalkanoic acid synthesis and biofilm formation in *Pseudomonas aeruginosa* by 2-bromoalkanoic acids: effect of inhibitor alkyl-chain-length. PLoS One. https://doi.org/10.1371/journal.pone.0073986.

Heipieper, H.J., Martínez, P.M., 2010. Toxicity of hydrocarbons to microorganisms. Handb. Hydrocarb. Lipid Microbiol. 1, 1563–1573. https://doi.org/10.1007/978-3-540-77587-4_108.

Jendrossek, D., 2009. Polyhydroxyalkanoate granules are complex subcellular organelles (carbonosomes). J. Bacteriol. 191, 3195–3202. https://doi.org/10.1128/JB.01723-08.

Jurasek, L., Marchessault, R.H., 2002. The role of phasins in the morphogenesis of poly (3-hydroxybutyrate) granules. Biomacromolecules 3, 256–261. https://doi.org/10.1021/bm010145d.

Kimura, N., Nishi, A., Goto, M., Furukawa, K., 1997. Functional analyses of a variety of chimeric dioxygenases constructed from two biphenyl dioxygenases that are similar structurally but different functionally. J. Bacteriol. 179, 3936–3943.

Kodama, K., Umehara, K., Shimizu, K., Nakatani, S., Minoda, Y., Yamada, K., 1973. Identification of microbial products from dibenzothiophene and its proposed oxidation pathway. Agric. Biol. Chem. 37, 45–50. https://doi.org/10.1271/bbb1961.37.45.

Li, M., Wang, T.G., Simoneit, B.R.T., Shi, S., Zhang, L., Yang, F., 2012. Qualitative and quantitative analysis of dibenzothiophene, its methylated homologues, and benzonaphthothiophenes in crude oils, coal, and sediment extracts. J. Chromatogr. A 1233, 126–136. https://doi.org/10.1016/j.chroma.2012.01.086.

Li, L., Shen, X., Zhao, C., Liu, Q., Liu, X., Wu, Y., 2019. Biodegradation of dibenzothiophene by efficient Pseudomonas sp. LKY-5 with the production of a biosurfactant. Ecotoxicology 176, 50–57. https://doi.org/10.1016/j.ecoenv.2019.03.070.

Lu, J., Tappel, R.C., Nomura, C.T., 2009. Mini-Review: biosynthesis of poly (hydroxyalkanoates). Polym. Rev. 49, 226–248. https://doi.org/10.1080/15583720903048243.

Ma, Z.-Q., Ma, Z., Dasari, S., Chambers, M.C., Litton, M.D., Sobecki, S.M., Zimmerman, L. J., Halver, P.J., Schilling, B., Drake, P.M., Gibson, B.W., Tabb, D.L., 2009. IDPicker 2.0: improved protein assembly with high discrimination peptide identification filtering. J. Proteome Res. 8, 3872–3881. https://doi.org/10.1021/pr900360j.

Nzila, A., Ramirez, C.O., Musa, M.M., Sankara, S., Basheer, C., Li, Q.X., 2018. Pyrene biodegradation and proteomic analysis in *Achromobacter xylosoxidans*, PY4 strain. Int. Biodeterior. Biodegrad. 130, 40–47. https://doi.org/10.1016/j.ibiod.2018.03.014.

Obruca, S., Sedlacek, P., Koller, M., 2021. The underexplored role of diverse stress factors in microbial biopolymer synthesis. Bioresour. Technol. 326, 124767. https://doi.org/10.1016/j.biortech.2021.124767.

Ortega Ramirez, C.A., Kwan, A., Li, Q.X., 2020. Rhamnolipids induced by glycerol enhance dibenzothiophene biodegradation in *Burkholderia* sp. C3. Engineering 6, 533–540. https://doi.org/10.1016/j.eng.2020.01.006.

Patowary, K., Patowary, R., Kalita, M.C., Deka, S., 2017. Characterization of biosurfactant produced during degradation of hydrocarbons using crude oil as sole source of carbon. Front. Microbiol. 8, 1–14. https://doi.org/10.3389/fmicb.2017.00279.

Piccoli, S., Andreolli, M., Giorgetti, A., Zordan, F., Lampis, S., Vallini, G., 2014. Identification of aldolase and ferredoxin reductase within the dbt operon of *Burkholderia fungorum* DBT1. J. Basic Microbiol. 54, 464–469. https://doi.org/10.1002/jobm.201200408.

Pini, C.V., Bernal, P., Godoy, P., Ramos, J.L., Segura, A., 2009. Cyclopropane fatty acids are involved in organic solvent tolerance but not in acid stress resistance in *Pseudomonas putida* DOT-T1E. Microb. Biotechnol. 2, 253–261. https://doi.org/10.1111/j.1751-7915.2009.00084.x.

Rehm, BH a, Mitsky, T.a., Steinbüchel, A., 2001. Role of fatty acid de novo biosynthesis in polyhydroxyalkanoic acid (PHA) and rhamnolipid synthesis by Pseudomonads: establishment of the transacylase (PhaG)-mediated pathway for PHA biosynthesis in *Escherichia coli*. Appl. Environ. Microbiol. 67, 3102–3109. https://doi.org/10.1128/AEM.67.7.3102-3109.2001.

Seo, J.-S., Keum, Y.-S., Li, Q.X., 2009. Bacterial degradation of aromatic compounds. Int. J. Environ. Res. Publ. Health 6 (1), 278–309. https://doi.org/10.3390/ijerph6010278.

Seo, J., Keum, Y., Li, Q.X., 2011. Comparative protein and metabolite profiling revealed a metabolic Network in response to multiple environmental contaminants in. J. Agric. Food Chem. 2876–2882.

Seo, J.S., Keum, Y.S., Hu, Y., Lee, S.E., Li, Q.X., 2007. Degradation of phenanthrene by *Burkholderia* sp. C3: initial 1,2- and 3,4-dioxygenation and meta- and ortho-cleavage of naphthalene-1,2-diol. Biodegradation 18, 123–131. https://doi.org/10.1007/s10532-006-9048-8.

Seo, J.S., Keum, Y.S., Li, Q.X., 2013. Metabolomic and proteomic insights into carbaryl catabolism by Burkholderia sp. C3 and degradation of ten N-methylcarbamates. Biodegradation 24, 795–811. https://doi.org/10.1007/s10532-013-9629-2.

Szulc, A., Ambrozewicz, D., Sydow, M., Ławniczak, Ł., Piotrowska-Cyplik, A., Marecik, R., Ł, Chrzanowski, 2014. The influence of bioaugmentation and biosurfactant addition on bioremediation efficiency of diesel-oil contaminated soil: feasibility during field studies. J. Environ. Manag. 132, 121–128. https://doi.org/10.1016/j.jenvman.2013.11.006.

Tabb, D.L., Fernando, C.G., Chambers, M.C., 2008. MyriMatch:highly accurate tandem mass spectral peptide identificaiton by multivariate hypergeometric analysis. J. Proteome Res. 6, 654–661. https://doi.org/10.1021/pr0604054.MyriMatch.

Tittabutr, P., Cho, I.K., Li, Q.X., 2011. Phn and Nag-like dioxygenases metabolize polycyclic aromatic hydrocarbons in *Burkholderia* sp. C3. Biodegradation 22, 1119–1133. https://doi.org/10.1007/s10532-011-9468-y.

Tyagi, M., da Fonseca, M.M.R., de Carvalho, C.C.C.R., 2011. Bioaugmentation and biostimulation strategies to improve the effectiveness of bioremediation processes. Biodegradation 22, 231–241. https://doi.org/10.1007/s10532-010-9394-4.

Venkateswar Reddy, M., Mawatari, Y., Yajima, Y., Seki, C., Hoshino, T., Chang, Y.C., 2015. Poly-3-hydroxybutyrate (PHB) production from alkylphenols, mono and poly-aromatic hydrocarbons using *Bacillus* sp. CYR1: a new strategy for wealth from waste. Bioresour. Technol. 192, 711–717. https://doi.org/10.1016/j.biortech.2015.06.043.

Wackett, L.P., 1996. Co-metabolism: is the emperor wearing any clothes? Curr. Opin. Biotechnol. 7, 321–325. https://doi.org/10.1016/S0958-1669(96)80038-3.